Glycol Porphyrin Derivatives as Potent Photodynamic Inducers of Apoptosis in Tumor Cells

Jarmila Králová,*[,†] Tomáš Bříza,[‡] Irena Moserová,[†] Bohumil Dolenský,[‡] Petr Vašek,[‡] Pavla Poučková,[§] Zdeněk Kejík,[‡] Robert Kaplánek,[‡] Pavel Martásek,[§] Michal Dvořák,[†] and Vladimír Král[‡,||]

Institute of Molecular Genetics, Academy of Sciences of the Czech Republic, Videnska 1083, 142 20 Prague 4, Czech Republic, Institute of Chemical Technology, Technicka 5, 166 28 Prague 6, Czech Republic, First Faculty of Medicine, Charles University in Prague, Katerinska 32, 121 08 Prague 2, Czech Republic, and Zentiva Research & Development, U Kabelovny 130, 10237 Prague 10, Czech Republic

Received February 28, 2008

The design and synthesis of glycol-functionalized porphyrins that contain one to four low molecular weight glycol chains that are linked via ether bonds to the meta-phenyl positions of *meso*-tetraphenylporphyrin and the comparison of fluorinated and nonfluorinated para derivatives are reported. The cellular uptake and photodynamic activity significantly depend on terminal groups of the glycol substituent. Hydroxy glycol porphyrins, in contrast with methoxy glycol porphyrins, show efficient intracellular transport and a high induction of apoptosis in tumor cell lines in vitro. Furthermore, the ethylene glycol chain at the meta position exhibits a superior efficacy that leads to the permanent ablation of human breast carcinoma (MDA-MB-231) in nude mice. In addition, fluorination enhanced the photosensitizing potential of para-phenyl derivatives. The analysis of the cell-death mechanism revealed that glycol-functionalized porphyrins represent novel nonmitochondrially localized photosensitizers that have a profound ability to induce apoptosis in tumor cells that act upstream of caspase activation. The strong interaction with a tumor marker (sialic acid) indicates the preferential association of these compounds with tumor cells.

Introduction

Apoptosis, or programmed cell death, is the key pathway in animal development and in tissue homeostasis.[1] It is also the standard pathway for the clearance of defective or aged cells in the body. This form of active death is very different from necrosis, which results in an uncontrolled bursting of cells followed by an inflammatory reaction.[2] Two general pathways for apoptotic cell death have been characterized. The extrinsic pathway is triggered by the ligand-induced activation of death receptors at the cell surface. The intrinsic pathway results from an intracellular cascade of events that are mainly produced by cellular stress, in which mitochondrial permeabilization plays a crucial role.[3] Cellular stress may occur after exposure to radiation or chemicals or to viral infection. It might also be a consequence of growth factor deprivation or oxidative stress caused by free radicals. The sensitivity of cells to any of these stimuli can vary depending on a number of factors such as the expression of pro- and antiapoptotic proteins (e.g., the Bcl-2 proteins or the inhibitor of apoptosis proteins (IAPs[a])), the severity of the stimulus, and the stage of the cell cycle. Although there is a variety of initiating apoptotic stimuli, the execution/degradation phase is common to distinct types of apoptosis and is independent of the initiating stimulus. The common features of cell degradation are the disruption of the mitochondrial transmembrane potential, the activation of caspases, nuclear fragmentation (which is frequently accompanied by internucleosomal DNA fragmentation), the redistribution of phospholipids in the plasma membrane (externalization of phosphatidylserine), blebbing, and the formation of apoptotic bodies.[3]

Disabled apoptosis is a pathogenic event that contributes to oncogenesis and cancer progression.[4] Many anticancer drugs have been designed to act against this malfunction and kill the cells by restoring their programmed cell-death mechanism.[5−16]

The main problem in using some of these drugs is their low selectivity for cancer cells and their often high toxicity to the body.

In contrast with radiation therapy and chemotherapy, photodynamic therapy (PDT) has fewer adverse side effects and has a higher selectivity.[17,18] PDT is based on the production of reactive oxygen species, mainly singlet oxygen ($^1O_2$),[19] by a photosensitizer (PS) after light exposure.[20] This cytotoxic effector of PDT acts locally because of its short lifetime, and thus the PS-induced damage is mostly limited to the organelle into which the PS localizes.[21,22] The type of cell death that is caused by PDT (apoptosis vs necrosis) depends on a number of factors[23,24] including the type and size of the tumor, the PDT treatment conditions, and the type of PS[25] and its site of accumulation.[26] There is a continuous effort toward the development of very efficient PSs that preferentially accumulate in tumor cells.

Suitable PSs are porphyrins[27] that have a high selectivity for cancer cells and have light absorption in the visible range of the spectrum, which is made possible by the polyconjugated aromatic system. A limitation, however, is their high hydrophobicity. The problem of the low solubility and the low cellular uptake of the porphyrin core can be solved by the addition of hydrophilic substituents (e.g., hydroxyl,[28] sugar,[29] amino borate, sulfate,[30] phosphonate,[31] cyclodextrin,[32] peptide,[33] and PEG).[34] Many water-soluble porphyrins[29,32] showed strong affinities for cancer cells and showed high anticancer effects. The substitution of the PS core can also be used for the modulation of the photophysical properties and the adjustment of chemical char-

* To whom correspondence should be addressed. Tel: +420-241 063 392. Fax: +420-241 063 586. E-mail: kralova@img.cas.cz.
† Academy of Sciences of the Czech Republic.
‡ Institute of Chemical Technology.
§ Charles University in Prague.
|| Zentiva Research & Development.

[a] Abbreviations: PDT, photodynamic therapy; PS, photosensitizer; MAPK, mitogen-activated protein kinase; MKK, MAP kinase kinase; JNK, *c*-Jun N-terminal kinase; PARP, poly-(ADP-ribose)-polymerase; IAPs, inhibitor of apoptosis proteins; PI, propidium iodide; PEG, polyethylene glycol; PEGME, polyethylene glycol-modified enzymes; PBS, phosphate-buffered saline; mTHPP, *meso*-tetrahydroxyphenyl porphyrin; mTHPC, *meta*-tetrahydroxyphenyl chlorin; CLSM, confocal laser scanning microscopy; OPD, overall photodynamic dose.

10.1021/jm8002119 CCC: $40.75
Published on Web 09/13/2008

Scheme 1. Syntheses of Symmetrical Nonfluorinated Porphyrins **2**−**5**

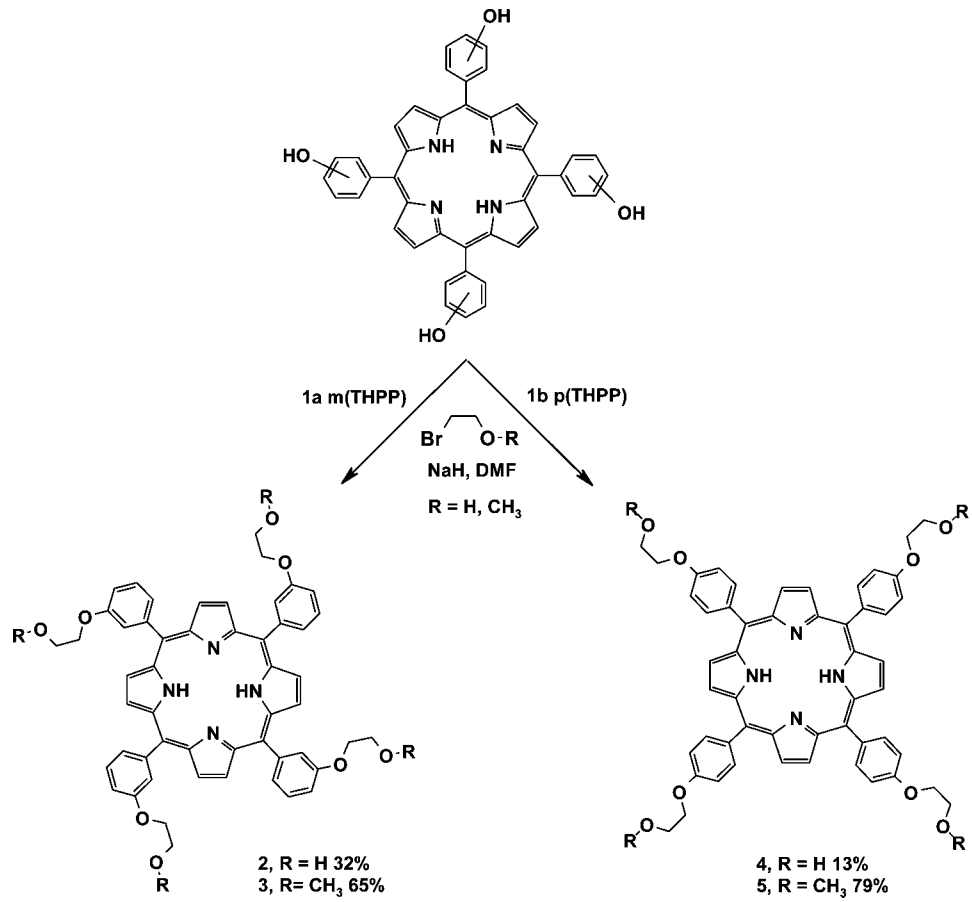

acteristics of the macrocycle. For example, these substituents can direct self-assembly[35] and target the PSs to therapeutically important objects (cancer cells,[36] mitochondria,[30] DNA[37]) or modulate their electronic properties[38] such as absorption and emission. Two types of these groups can be distinguished: ionic and nonionic. The electrical charge of the ionic groups affects the charge-mediated recognition of important cancer receptors such as sialic acid. Some nonionic hydrophilic groups such as PEG and PEGME can have an affinity for the cell membrane and can therefore be used for the facilitation of membrane entry.[39]

Another important modification of the PS core is fluorine substitution.[40] The incorporation of fluorine results in the modification of the pharmacodynamic and pharmacokinetic properties of the drugs; it increases their biological half-life by impeding oxidative metabolism and bioabsorption. Moreover, fluorinated porphyrins can be used for in vivo imaging by fluorescence spectroscopy and ^{19}F nuclear magnetic resonance spectroscopy.[41] New theories such as polar hydrophobicity[42] help to explain the increased binding of fluorinated molecules to proteins. Selective interactions with specific amino acid residues in a binding site have been described.[43]

As a part of our continuing studies of the structure/activity relationship and the biological efficacy of porphyrin-based PSs, we report here the synthesis of a series of nonionic porphyrins with glycol peripheral substitutions. The main idea behind our design is to improve the solubility, the bioavailability, and the biological performance of the already known PS, tetra-hydroxyphenyl-porphyrin, by the introduction of a monoethylene glycol moiety. We have also studied the effect of fluorination, the position of the substitution, and the influence of terminal groups. In vitro studies show that the extent of the cellular uptake of the derivatives depends significantly on the terminal groups of a glycol substituent and it correlates with the induction of apoptosis after PDT. The position of glycol substituents (meta or para) affects the intracellular localization and the PDT efficacy. We demonstrate that the presence of fluorine atoms endows the *para*-ethylene glycol porphyrin with better biological virtue. The signal pathways that are involved in apoptosis are induced by various glycol porphyrin derivatives that resemble those that are induced by the tetrakis-*meso*-(4-ethyleneglycol-2,3,5,6-tetrafluorophenyl) porphyrin that was recently described in detail.[44] Therefore, neutral and highly water-soluble glycol porphyrin derivatives are very potent inducers of apoptosis in tumor cells that have a high potential for in vivo PDT applications. Their strong interaction with sialic acid might be a basis for tumor-cell recognition.

Results and Discussion

Synthesis of the Porphyrins. Two types of meso-tetrasubstituted porphyrins were prepared and tested.

The first type, which comprised nonfluorinated derivatives **2**−**5** (Scheme 1), consists of the porphyrins that were substituted by monoethylenene glycol chains. The glycol units that were used for the substitution of the porphyrins were composed of two types of monoethyleneglycol chains: one with the terminal hydroxy group and the other with the terminal methoxy group. The glycol chains were anchored at para or meta positions of meso-phenyl groups (Schemes 1 and 3). Their synthesis was based on the nucleophilic substitution of tetrakis-5,10,15,20-(4-hydroxyphenyl)porphyrin and tetrakis-5,10,15,20-(3-hydroxyphenyl)porphyrin, respectively, with a suitable bromo deriva-

Scheme 2. Syntheses of Symmetrical Fluorinated Porphyrins **6**−**9**

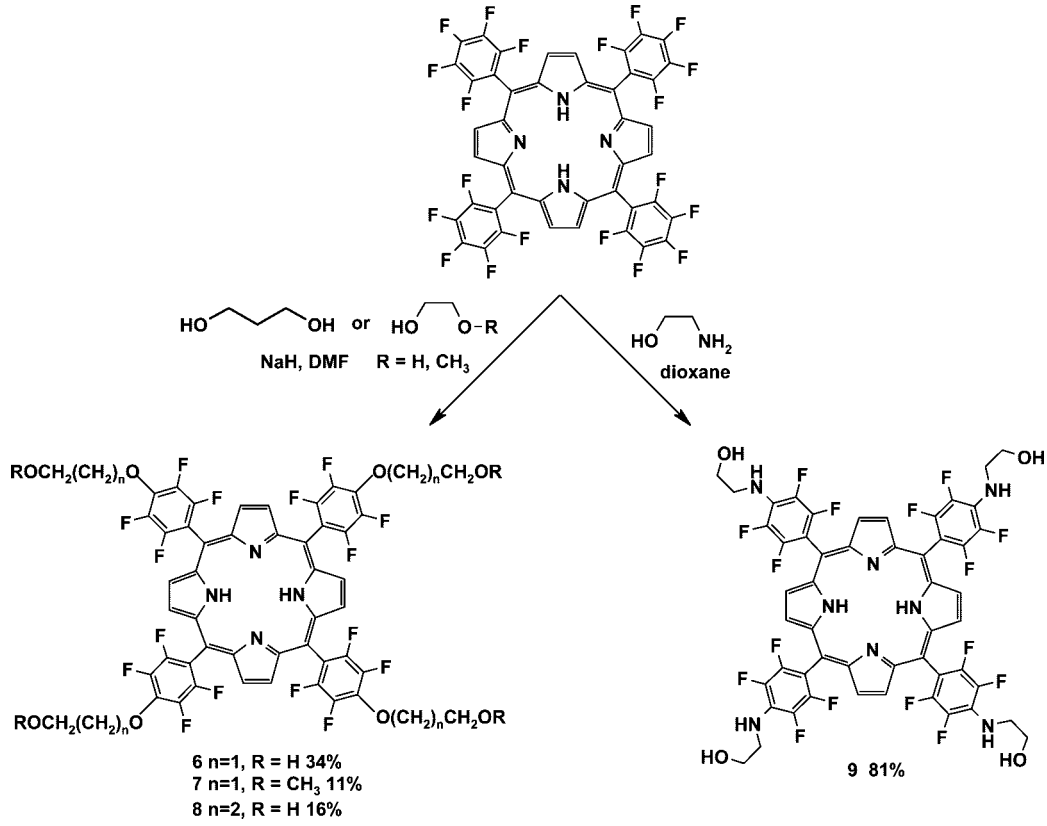

Scheme 3. Syntheses of Asymmetrical Nonfluorinated Porphyrins **10**−**12**

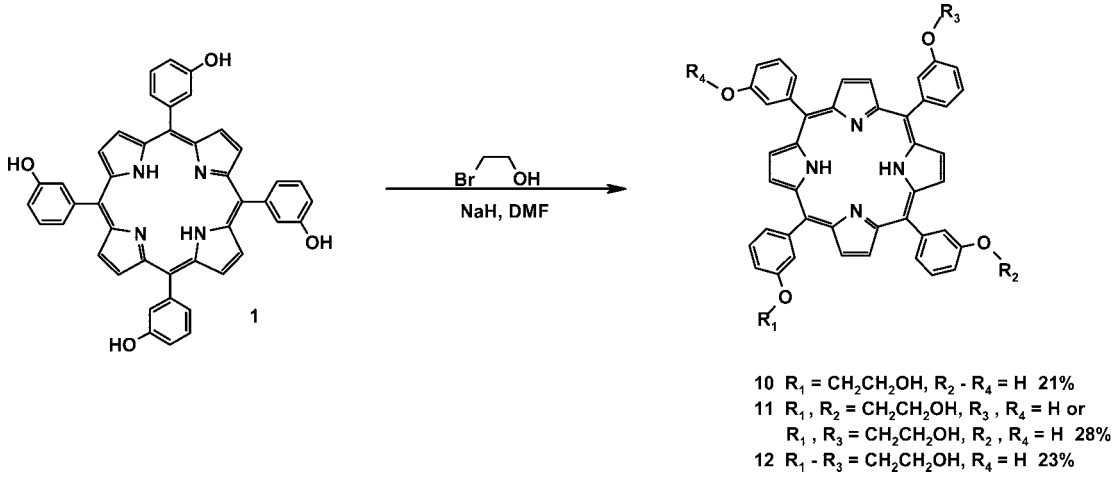

tive (either 2-bromoethanol or 2-bromo-1-methoxyethane (Schemes 1 and 3)). Optimal reaction conditions were as follows: (1) in the case of symmetrical tetra-substituted derivatives **2**−**5**, the hydroxyporphyrins were reacted with an excess of the corresponding bromo derivatives in the presence of potassium carbonate in dimethylformamide under heating, (2) in the case of asymmetrical derivatives **10**−**12** (Scheme 3) with terminal −OH groups, the hydroxyporphyrin was reacted with 4 equiv of 2-bromoethanol under conditions mentioned above, and (3) the individual derivatives **10**, **11**, and **12** were separated by means of column chromatography. Symmetrical porphyrin derivatives **2** and **4**, with a terminal −OH group on the glycol chain, were formed in 32 and 13% yield, respectively. Asymmetrical derivatives **10**−**12** were formed in 20% average yield. Derivatives **3** and **5,** with terminal methoxy groups on glycol chains, were formed in 65 and 79% yield, respectively.

The second type of meso-tetrasubstituted porphyrins, which is represented by fluorinated derivatives **6**−**8** (Scheme 2), was prepared by the substitution in para positions of meso-pentafluorophenyl groups with either monoethylene glycol or monopropylene glycol chains (Scheme 2). At first, sodium or lithium salts were generated from corresponding glycols ethane-1,2-diol, propane-1,3-diol, and 2-methoxyethan-1-ol by sodium hydride or by LDA in dimethylformamide at laboratory temperature. Then, tetrakis-5,10,15,20-(pentafluorophenyl)porphyrin was added, and the mixture was stirred under heating. Products **6**−**8** were formed in 11−34% yield (Scheme 2). Porphyrin derivative **9** with side chains connected to porphyrin fluorophe-

Table 1. Concentration of Porphyrin Derivatives and Overall Photodynamic Dose Required for 50% Inhibition of the Cell Viability

	HL60		4T1	
derivative	IC_{50} (nM) ± SD[a]	OPD[b]	IC_{50} (nM) ± SD	OPD
1a[c]	126 ± 5	312	200 ± 40	500
1b[c]	660 ± 30	2500	1050 ± 50	3990
2[c]	42 ± 5	105	110 ± 8	275
3[c]	NE[e]	NE		
4[c]	2000 ± 130	5000	2200 ± 240	5500
5[c]	NE	NE		
6[c]	150 ± 30	375	200 ± 20	500
7[c]	NE	NE		
8[c]	5300 ± 240	13 250	6500 ± 160	16 260
9[c]	2200 ± 160	5500	2600 ± 80	6500
10[c]	93 ± 10	232	143 ± 6	358
11[c]	33 ± 5	83	95 ± 12	238
12[c]	31 ± 7	78	93 ± 7	233
mTHPC[d]	42 ± 8	559	117 ± 71	1556

[a] Values represent the mean ± SD of three to six replicated experiments. [b] Overall photodynamic dose (drug dose × light dose). [c] Exposed to 500−520 nm light (light dose 2.5 J/cm^2 for **1a** and **2**−**12** and 3.8 J/cm^2 for **1b**). [d] Exposed to 620−660 nm light (light dose 13.3 J/cm^2). [e] NE is not effective at concentrations ≤10 μM.

nyl groups via a nitrogen atom was also prepared. The synthesis was based on the reaction of 2-aminoethanol with pentafluorophenyl porphyrin under heating. The product was formed in 81% yield (Scheme 2).

Biological Data. Intracellular Localization. The effect of the variation of peripheral glycol chain number, length, and position on the intracellular concentration and distribution was determined by the fluorescence of porphyrin derivatives **2**−**12** in 4T1 cells. The porphyrins (0.5−10 μM) were added to the medium, and cells were analyzed 2, 4, and 16 h later by fluorescence microscopy. No principal temporal redistribution of the fluorescence pattern of any compound was observed. Compounds **2** and **10**−**12** exhibited diffuse fluorescence throughout the cytoplasmic area within 2 h, whereas **4**, **6**, **8**, and **9** displayed the characteristic punctuated pattern with increasing intensity after prolonged incubation (exemplified by **2** and **6** in the Supporting Information (Figure 1)). The fluorescence of parent compounds mTHPP (**1a**) and pTHPP (**1b**) was weaker, and it showed delayed kinetics in comparison with glycol derivative **2**. In contrast, methoxy glycol porphyrins **3**, **5**, and **7** did not show any significant intracellular fluorescence (not shown), which indicates their poor cellular uptake that leads to very low biological activity (Table 1). Therefore, they were not included in further investigations.

However, it is not only the cellular uptake but also the distribution of PSs inside the cell that is important for its phototoxic activity. To identify the intracellular compartment where derivatives had accumulated, we costained cells with fluorescent LysoTracker Green, MitoTracker Green, and ER-Tracker Blue-White probes, and we analyzed cells by confocal microscopy (Figure 1; Supporting Information (Figure 2)). None of the compounds had accumulated in mitochondria. (See the Supporting Information.) The costaining with LysoTracker Green revealed that all para derivatives **4**, **6**, **8**, and **9** accumulated in a subset of LysoTracker-stained structures. Fluorination had no observable effect on the localization (compare panels for **4** and **6**). In contrast, similar to the parental tetrahydroxyphenyl porphyrin (mTHPP (**1a**)), all meta derivatives with one (**10**), two (**11**), three (**12**), and four (**2**) ethylene glycol chains exhibited strong colocalization with the ER-Tracker Blue-White probe (Figure 1; Supporting Information (Figure 2)). Importantly, in comparison with ethylene glycol-functionalized porphyrins, mTHPP (**1a**) displayed a lower

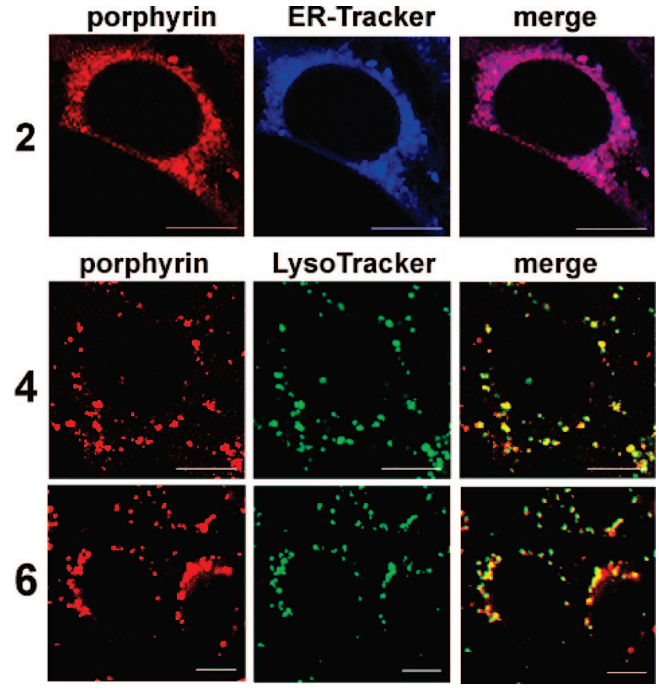

Figure 1. Subcellular localization of glycol porphyrin derivatives determined by confocal laser scanning microscopy (CLSM). 4T1 cells were sequentially loaded with porphyrins and specific probes for endoplasmic reticulum and lysosomes. Porphyrin fluorescence (red) is shown in the left panels, ER-Tracker fluorescence (blue) or LysoTracker fluorescence (green) is shown in the middle panels, and an overlay of ER-Tracker or LysoTracker fluorescence with porphyrin fluorescence is shown in the right panels. Colocalication is pink and yellow/orange, respectively. Used concentrations of derivatives are given in the Experimental Section. Scale bars: 10 μM.

intensity of intracellular fluorescence, which, after prolonged incubation, partially affiliated with a subset of LysoTracker-stained structures and thereby indicated the formation of aggregates that were entrapped in this compartment (Supporting Information (Figure 2: left column, third panel)).

Therefore, the localization pattern of the porphyrin derivatives inside the cells seems to be affected mainly by the position of ethylene glycol chains. Similar observations have been published for glycoconjugated porphyrins.[45]

In Vitro Phototoxicity. To investigate the photodynamic potential of the glycol porphyrin derivatives, we incubated two cell lines (human promyelocytic leukemia HL60 and mouse mammary carcinoma 4T1) with increasing concentrations of the porphyrins for 16 h and then illuminated them with filtered light (500−520 nm, 2.5 J/cm^2). Cells that were incubated with the porphyrins without illumination (dark control) were kept in parallel. Following the illumination of the cell lines, the viability of post-PDT cultures was determined the next day by the Trypan blue exclusion method, and dose/response curves were obtained. The IC_{50} values, which represent the concentration of the porphyrins that is required to kill 50% of cells, were calculated for each curve, and they are summarized in Table 1. Porphyrin **2** with symmetrical ethylene glycol substitutions in all four meta-phenyl positions was able to evoke IC_{50} in HL60 and 4T1 cells at 47- and 20-fold lower concentrations, respectively, than the corresponding derivative **4** with glycol chains in the para position (Table 1). A similar impact of position on activity has been described for chlorins.[28] Fluorinated para-substituted porphyrin **6** showed an increased biological efficacy in comparison with its unfluorinated analog **4**. Such enhancement of biological activity by fluorination might indicate better molecular

targeting of the whole molecule, which is likely due to the noncovalent hydrophobic interaction of the aromatic macrocycle with the aromatic region of biopolymers and the selective interaction with lipophilic domains.[42] However, in the case of fluorinated para-substituted porphyrins, both the elongation of the glycol chains (**8**) and the substitution of nitrogen for oxygen (**9**) weakened the biological activity of the resulting compound, which thereby indicates a delicate influence of various factors on the biological activity of the synthesized porphyrin derivatives.

The data that were obtained under the same experimental conditions as those for the parent *meta*-tetrahydroxyphenyl porphyrin (mTHPP (**1a**)) and *para*-tetrahydroxyphenyl porphyrin (mTHPP (**1b**)) including tetrahydroxyphenyl chlorine (mTHPC), an active compound of the marketed drug Foscan, were included for comparison (Table 1; Supporting Information (Figures 1 and 2)). It is obvious that para-substituted THPP behaves differently than meta-substituted THPP. Furthermore, although active concentrations of mTHPC fall within a range that is similar to that of the glycol porphyrins, the used optimal wavelengths filters, 650 and 500 nm, respectively, provided different light intensities (3.7 and 0.7 mW/cm^2, respectively) and resulting light doses (13.3 and 2.5 J/cm^2, respectively). Therefore, the overall photodynamic dose (drug dose × light dose) that is required to reach IC_{50} was about 5 times lower for *meta*-ethylene glycol-functionalized porphyrin **2** than for mTHPC, which shows the superior potency of **2**.

A detailed study of PEG-functionalized *meso*-tetraphenylporphyrins has been published recently.[34] Conjugates of porphyrins that have hexaethylene glycol in the para position have shown that the cellular properties of the PEG-substituted porphyrins depend on the number of PEG chains that are linked to the porphyrin ring. The better cellular uptake and phototoxicity of the mono-PEG and the adjacent di-PEG substitution at the porphyrin periphery were ascribed to their amphiphilic character. In contrast with that study, when we introduced various numbers of ethylene glycol chains to the meta position, the resulting asymmetric mono, bis, and tris derivatives (**10**, **11**, and **12**) did not show such a relation. The number of ethylene glycol chains substantially affected neither the intracellular localization (Supporting Information (Figure 2)) nor the in vitro PDT efficacy (Table 1). Conversely, the best PDT efficacy was achieved with tris-substituted derivative **12**. It is generally accepted that peripheral substitutions play an important role in the biological availability and activity of the compound. Our results suggest that porphyrins with ethylene glycol functionalities in the meta position displayed a 1.4- to 4-fold better PDT efficacy than did parent tetrahydroxyphenyl porphyrin mTHPP (**1a**) (Table 1). Moreover, *meta*-ethylene glycol derivatives, in terms of the overall photodynamic dose (drug dose × light dose), displayed a 5.5- to 19-fold higher cytotoxic effect than did the best reported PEG-substituted porphyrin ($IC_{50} = 2\ \mu$M at 1 J/cm^2).[34]

According to the results that are presented in Table 1, Figure 1, and the Supporting Information (Figures 1 and 2), the correlation between the cellular uptake of the porphyrins and their photobiological efficacy is evident. Generally, the porphyrins with rather high cell-penetration efficiency (**2**, **4**, **6**, **8**, and **9**) displayed high phototoxic activity, whereas poorly penetrating porphyrins (**3**, **5**, and **7**) were inefficient. Lower photodynamic activities have also been reported for methoxy-substituted arylporphyrins with respect to hydroxyl derivatives,[46] but the difference has not been as striking as the one we found for glycol porphyrins. Furthermore, very effective derivatives **2**, **10**, **11**, and **12** mostly accumulated in the endoplasmic reticulum, whereas the localization in lysosomes, with the exception of **6**, resulted in a lower photodynamic efficacy (**4**, **8**, and **9**) (Table 1, Figure 1, and the Supporting Information (Figure 2)).

In addition, a further explanation of the unique photodynamic abilities of ethylene glycol porphyrins versus those of parent hydroxyphenyl porphyrin is based on their different aggregation properties, which were affected by the exchange of the phenolic terminal group for the alcoholic terminal group. The parent hydroxy porphyrin **1a** exhibited a strong tendency to aggregate in the lower pH 6, which was demonstrated by a decrease in absorbance that is obvious from the spectral analysis of its aqueous solutions (Supporting Information (Figure 5)). In contrast, ethylene glycol derivatives **2**, **11**, and **12** did not show such behavior in response to the relevant physiological pH (Supporting Information (Figures 5 and 6)), and they are therefore more favorable PSs. These spectral characteristics correlate with intracellular fluorescence data (Supporting Information (Figures 1 and 2)) and are consistent with biological performance (Table 1) because lower aggregation translates into higher photodynamic efficacy.

To the best of our knowledge, we demonstrate here for the first time such a dramatic enhancement of PDT efficacy just by a simple ethylene glycol substitution on the porphyrin periphery.

Glycol Porphyrin Derivatives Kill Cells by Apoptosis. There are many reports that describe that cells that are exposed to PDT might die by a regulated process, apoptosis. Here we found that glycol-functionalized porphyrins are potent PSs that have the capacity to initiate apoptosis in both suspension and adherent cancer cells. To study the mode of cell death, we selected the optimal concentration of each derivative to kill 50−80% cells at a low light dose (2.5 J/cm^2). A hallmark of apoptosis is the change in membrane permeability that is demonstrated by phosphatidylserine externalization on the outer leaflet of the plasma membrane, which is an early feature of apoptotic cells. The apoptosis determination was conducted by the dual fluorescence of Annexin V-FITC/PI and was measured by flow cytometry to distinguish necrotic, apoptotic, and live cells. HL60 cells were treated with **2**, **4**, **6**, **8**, and **9** overnight, and 4.5−6.5 h after illumination, they were stained with Annexin V and PI. As shown in Figure 2, the percentage of Annexin-positive cells slightly varied depending on the derivative. Kinetic studies showed that in an early stage after PDT treatment only a few cells were positive with either Annexin or PI. However, with time progression (4−6 h), large portions of cells that were stained with Annexin (early apoptotic cells) later (>5 h) also became PI-positive (late apoptotic cells). Therefore, the total percentage of apoptotic cells is considered to be the sum of early apoptotic cells (B4) and late apoptotic cells (B2), that is, B2 + B4. Photoactivation seems to be an ultimate requirement for the induction of apoptosis because control cells without illumination (Figure 2, panel C) did not show significant cell death. From these results, it could be concluded that all of the the derivatives induced apoptosis extensively at selected concentrations.

To further confirm the apoptotic phenotype of HL60 and 4T1 cells, we examined another biochemical hallmark of apoptosis. The integrity of the DNA that was isolated from cells that were exposed to photosensitization was studied by gel electrophoresis. In both cell types that were exposed to **2**-, **4**-, **6**-, **8**-, and **9**-mediated PDT, pronounced DNA fragmentation was detectable within 3 to 4 h after illumination (Figure 3). In contrast, the DNA of control cells that were incubated with the PS without illumination remained intact.

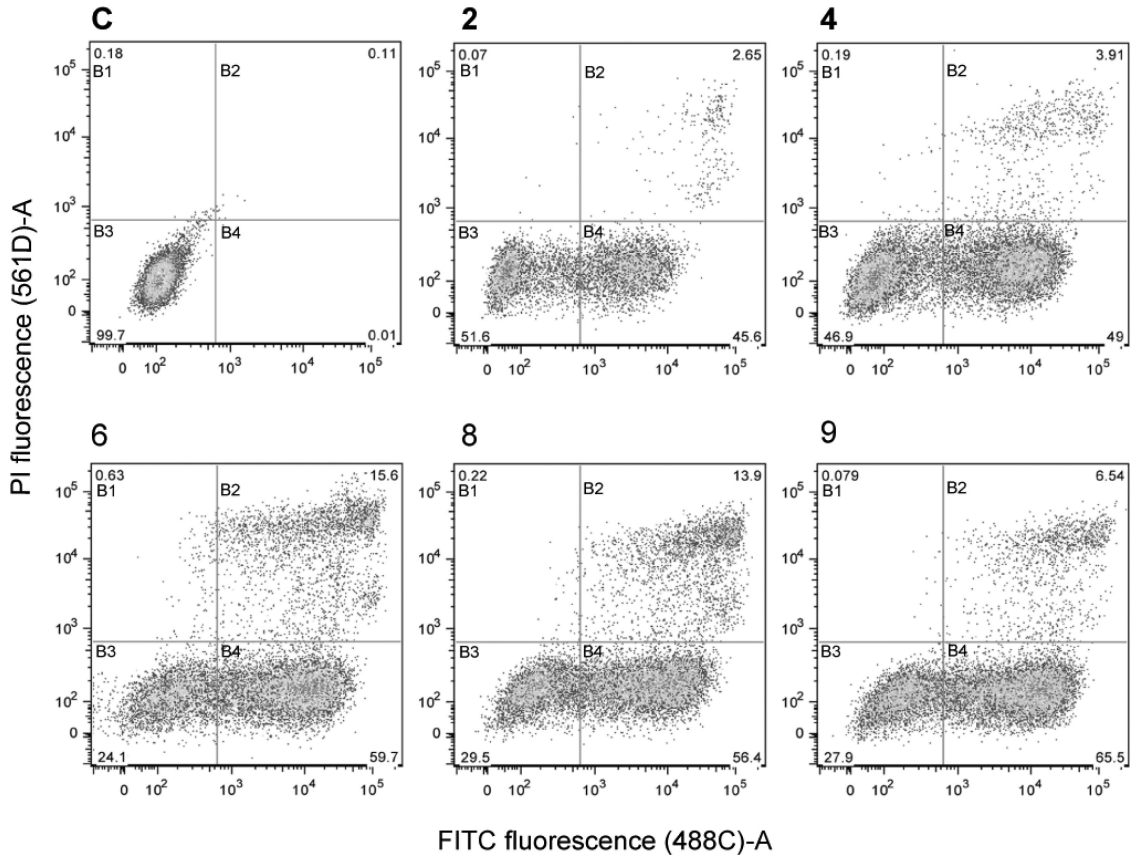

Figure 2. Apoptosis detection in HL60 cells by the use of the Annexin V assay. Cells were treated with glycol porphyrin derivatives **2** (180) nM), **4** (3 μM), **6** (300 nM), **8** (6.5 μM), and **9** (2.2 μM) overnight and were illuminated with 500−520 nm light (2.5 J/cm^2, 0.7 mW/ cm^2). Following incubation in the dark (**2** for 4.5; **4** for 6.5; and **6**, **8**, and **9** for 5.5 h), cells were stained with Annexin V and propidium iodide (PI) and were analyzed by flow cytometry. The total percentage of apoptotic cells is the sum of early apoptotic cells that were positive for Annexin V-FITC (B4) and late apoptotic cells that were stained with Annexin and PI (B2). Control cells (C) were treated with porphyrin without illumination.

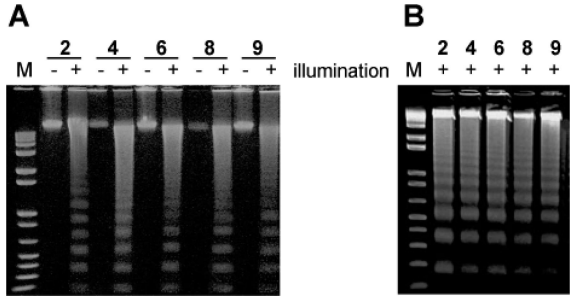

Figure 3. DNA fragmentation in 4T1 (A) and HL60 cells (B) that were exposed to PDT with glycol porphyrin derivatives. Cells were treated with **2** (300−350 nM), **4** (3−4 μM), **6** (500−600 nM), **8** (5−6 μM), and **9** (2−2.5 μM) for 16 h, were illuminated (2.5 J/cm^2), and were subsequently cultured in fresh medium for 3 to 4 h. In control cells, the illumination step was omitted (−). After harvesting, the DNA fragmentation was analyzed by 1.5% agarose gel electrophoresis. M is the DNA marker.

Apoptosis is characterized as an ordered process in which multiple events take place including post-translation modifications of key regulatory molecules such as protein kinases, Bcl-2 family members, and caspases. To investigate intracellular signaling events that are set in motion in cells that are photosensitized with various glycol porphyrin derivatives, we analyzed the protein profile of several important players by Western blot analysis (Figure 4). In our recent study, we have described the importance of the p38 MAP kinase signaling mechanism for the induction of apoptosis in various tumor cell lines by **6**.[44] Here an analogous study was performed simultaneously for all derivatives to find out whether there is a correlation among the chemical structures of the PSs and their intracellular localization and the signaling pathways that are activated by photoactivation. Despite the differences in the structure of the glycol porphyrin derivatives and their PDT efficacy (Table 1), very similar pathways that lead to apoptosis were activated (Figure 4). The activation of the p38 MAP kinase pathway, including that of upstream kinases MKK3/6, which was demonstrated by their phosphorylation (P-MKK3/6, P-p38), was found to be much higher in cells that were exposed to photosensitization than in nonilluminated controls. Although the activation of JNK kinase seems profound, its relevancy for the induction of apoptosis has not been proven in our previous study.[44] Furthermore, in cells that undergo photoinduced apoptosis, the levels of antiapoptotic Bcl-2 and Mcl-1 proteins were reduced and caspase-3, -8, and -9 were activated (which was demonstrated by their proteolytic cleavage, indicated by an arrow) including the cleavage of the caspase-3 target, PARP. Surprisingly, **2** localized mostly in the endoplasmic reticulum, which activated molecular events that were similar to those of predominantly lysosomally localized **4**, **6**, **8**, and **9**. It is generally accepted that there is a strong correlation between the cell-death mechanism and primary photodamage sites, which are determined by the intracellular localization of the PS.[47] It is likely that glycol functionalities not only impart water solubility to the porphyrin core but also favor the binding to molecular targets that either are common in both cellular compartments or are different but lead to the activation of similar pathways. The identification of molecular targets for **2** and **6**

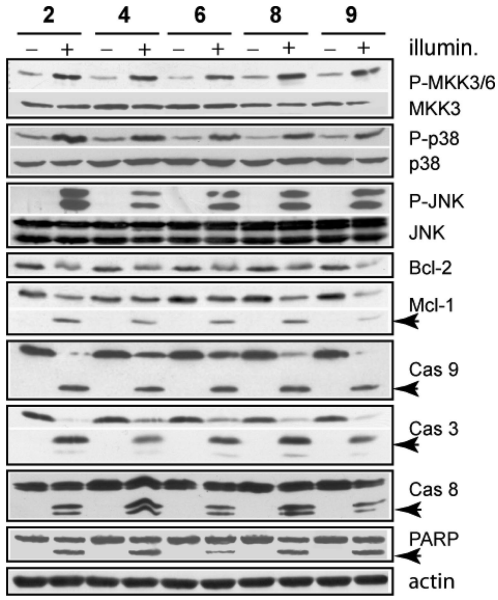

Figure 4. Induction of apoptosis in HL60 cells by glycol porphyrin derivatives demonstrated by the activation of MAP kinases, caspases, and changes in the Bcl-2 family. Cells that were treated with derivatives were exposed to the light (2.5 J/cm^2) (+), and they were harvested 2 h post-PDT. Whole cell lysates were analyzed by Western blot analysis. Control samples that run in parallel represent lysates from cells in which the illumination step was omitted (−). The kinase activity was determined by phospho-specific antibodies (P−) that were used at first (upper panel), and then the membrane was reprobed with antibodies to total MAPK (lower panel). The activated forms of caspases, cleaved Mcl-1 and PARP proteins, are labeled by arrows. Equal protein loading is demonstrated by actin reprobing.

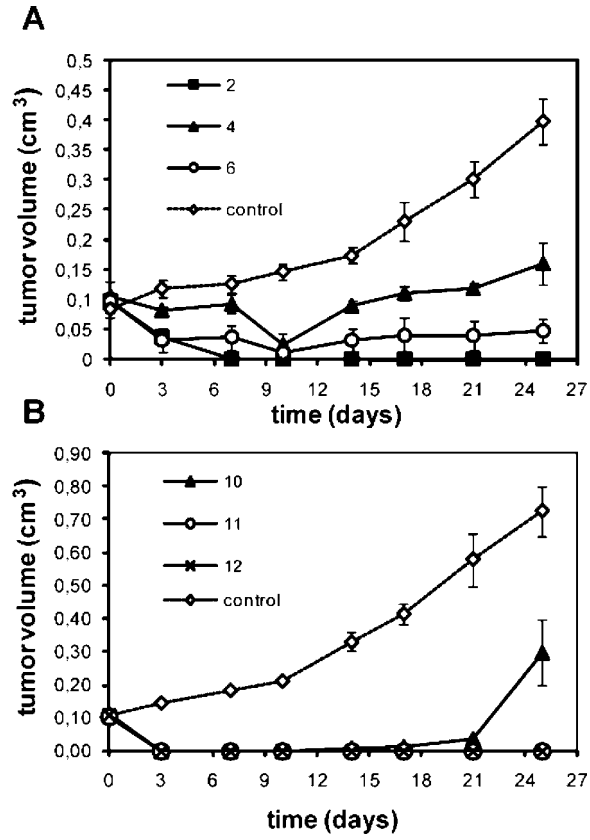

Figure 5. Effects of glycol-porphyrin-mediated PDT on tumor growth. Nude mice (NuNu) bearing subcutaneously growing human breast carcinoma MDA-MB-231 ($n = 5$ per each group) received an iv. dose of the drug (3 mg/kg), and after 2 h for **2**, **4**, **6**, **10**, **11** and after 6 h for **12**, tumor areas were illuminated with light (100 J/cm^2). After 1 week, the PDT treatment was repeated. The control group consisted of mice that were exposed to illumination without PS application. The tumor size was measured repeatedly and the tumor volume was determined. A and B summarize the results from two different experiments.

will be of great importance in the search for triggers of apoptotic signals. Experiments in such a direction are in progress.

We believe that the cell recognition that is based on tumor-marker selective binding of PSs as well as an understanding of the signaling mechanisms may provide a means to modulate PDT effects at the molecular level and to potentiate its antitumor effectiveness.

In Vivo PDT Efficacy. Porphyrins **2**, **4**, **6**, and **10**−**12** were selected for in vivo analysis to define their PDT effectiveness. NuNu mice bearing human breast carcinoma MDA-MB-231 received the respective PS (3 mg/kg iv), and tumors were illuminated (100 J/cm^2) at various time intervals after drug administration. The application of the drugs and illumination were repeated 1 week later, and afterward, tumor size was regularly measured. Here we present results for the 2 or 6 h interval in which the maximal tumor growth reduction was recorded (Figure 5A,B). In mice that were treated with **2**, **11**, and **12**, all tumors were completely eliminated with no detectable relapse of primary tumor. In contrast, animals that were treated with **4**, **6**, and **10** exhibited only transient tumor regression, and from day 10, primary tumors started to regrow gradually. Tumor relapse likely originated from a small population of tumor cells that survived PDT. The anticancer effects of PDT are thought to occur at two different levels: (1) direct lethal effects on tumor cells and (2) vascular impairment that limits blood supply to the region.[48] Future pharmacokinetic studies that use fluorescent intravital microscopy to determine the blood vessel perfusion and the accumulation of the drug in the interstitial compartment could determine their effect in the overall PDT efficacy.

Interaction with Sialic Acid. The high effectiveness of glycol porphyrin derivatives toward cancer cells led us to speculate that one of the important properties of these compounds might be the preferential association with biomolecules that is characteristic of cancer cells. We selected sialic acid as a well known example of a tumor marker that is localized on the cell surface, and we examined the selectivity of its binding with **2**, **4**, and **6**. A strong interaction that was demonstrated by titration experiments is shown for **6** (Figure 6; for **2** and **4** see Supporting Information (Figures 3 and 4)). The calculated binding constant pK_a (for 2:1 complexes) is 7.4, 8.2, and 10.1 for **2**, **4**, and **6**, respectively. Such strong interaction with sialic acid might have some biological relevancy by playing a role in cancer-cell recognition. This ability, together with the induction of apoptosis, suggests that a proper design of chemical structure (choice of substituents and their positions) might result in tailored substances that are able to target a specific cell type (cancer cells, in particular). To prove such a concept, further investigations and verifications in the context of the whole cell are needed.

Conclusions

The structure/activity relationship and the biological efficacy of porphyrin-based PSs were demonstrated on a series of low molecular weight glycol-functionalized *meso*-tetraphenylporphyrins. The cellular uptake of derivatives depends significantly on the terminal groups of the glycol substituent; only hydroxy glycol porphyrins **2**, **4**, **6**, **8**, and **9**−**12**, in contrast with methoxy glycol porphyrins **3**, **5**, and **7**, exhibit intracellular uptake and

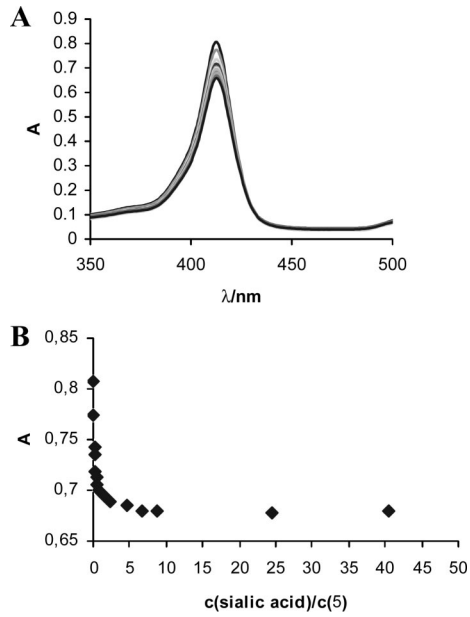

Figure 6. (A) Absorbance changes during the titration of **6** ($c = 2 \times 10^{-6}$ mol/L) with sialic acid at pH 5.5 (0.01 M phosphate buffer) in the presence of 15% PEG 400. (B) Titration curve of **6** with sialic acid at the maximum of absorbance (413 nm). Calculated pKas are 10.1. Stoichiometry of the complex (sialic acid/**6**) is 2:1.

phototoxicity. The bioavailability and efficacy was further determined by the glycol chain being in either the meta-phenyl or the para-phenyl position. Ethylene glycol in meta position (**2**, **10**−**12**) exhibited better intracellular uptake with predominant endoplasmic reticulum localization and superior PDT efficacy both in vitro and in vivo. The lower efficacy of para-analog **4** was improved by the fluorination of the phenyl ring (**6**). Our results show that, despite the differences in the cellular uptake, the phototoxicity, and the preferential sites of subcellular localization, glycol porphyrin derivatives are very potent inducers of apoptosis in tumor cells that assert tumor-marker recognition and act through a similar cell-death mechanism. A high potential of the *meta*-ethylene glycol derivatives for in vivo PDT applications is indicated.

Experimental Section

Synthesis of the Compounds. Compound 2. A flask was charged with 5,10,15,20-tetrakis(3-hydroxyphen-1-yl)porphyrin (30 mg, 44 μmol), potassium carbonate (100 mg, 0.72 mmol), 2-bromoethan-1-ol (100 mg, 0.80 mmol), and dimethylformamide (2 mL). The mixture was heated with stirring at 100 °C for 5 h. The mixture was evaporated, and the product was separated by means of column chromatography (silica, eluent methanol/dichloromethane 1:10). The product was obtained as a purple solid (12 mg, 32%). δ_H (300 MHz, $CDCl_3$): 2.82 (s, 2H), 2.14 (bs, 4H), 4.04 (bs, 8H), 4.28 (t, $J = 4.7$ Hz, 8H), 7.34 (dd, $J = 8.0$, $J = 2.2$ Hz, 4H), 7.64 (t, $J = 7.7$ Hz, 4H), 7.79 (s, 4H), 7.83 (d, $J = 7.7$ Hz, 4H), 8.87 (s, 8H). Anal. Calcd for $C_{52}H_{46}N_4O_8$: C, H, N.

Compounds 10−12. A flask was charged with 5,10,15,20-tetrakis(3-hydroxyphen-1-yl)porphyrin (250 mg, 0.37 mmol), potassium carbonate (250 mg, 0.37 mmol), 2-bromoethanol (185 mg, 1.48 mmol), and dimethylformamide (5 mL). The mixture was heated with stirring to 100 °C overnight. The mixture was evaporated, and the product was separated by means of column chromatography (silica, eluent diethyl ether/methanol 10:1). The first fraction contained monosubstituted product **10** (42 mg, 21%), the second fraction contained **11** (58 mg, 28%) and the third fraction contained **12** (51 mg, 23%). The individual products were obtained as purple solids. Compound **10**: δ_H (300 MHz, DMSO): 2.96 (s, 2H), 3.79 (t, 2H), 4.19 (t, 2H), 4.94 (t, $J = 5.2$ Hz, 1H), 7.23 (d, $J = 8.0$ Hz, 3H), 7.40 (d, $J = 7.7$ Hz, 1H), 8.89 (s, 8H), 9.90 (s, 3H). Anal. Calcd for $C_{46}H_{34}N_4O_5$: C, H, N. Compound **11**: δ_H (300 MHz, DMSO): 2.96 (s, 2H), 3.79 (t, 4H), 4.19 (t, 4H), 4.94 (t, $J = 5.2$ Hz, 2H), 7.23 (d, $J = 8.3$ Hz, 2H), 7.40 (d, $J = 8.3$ Hz, 2H), 8.89 (s, 8H), 9.92 (s, 2H). Anal. Calcd for $C_{48}H_{38}N_4O_6$: C, H, N. Compound **12**: δ_H (300 MHz, DMSO): 2.96 (s, 2H), 3.60 (t, $J = 4.7$ Hz, 6H), 4.19 (t, $J = 4.7$ Hz, 6H), 4.93 (t, $J = 5.2$ Hz, 3H), 7.23 (d, $J = 8.3$ Hz, 1H), 7.40 (d, $J = 8.3$ Hz, 3H), 8.89 (s, 8H), 9.91 (s, 2H). Anal. Calcd for $C_{50}H_{42}N_4O_7$: C, H, N.

The syntheses of other compounds are described in the Supporting Information.

Cell Cultures. Cell lines HL60 (human promyelocytic leukemia), 4T1 (mouse mammary carcinoma), and MDA-MB-231 (human breast carcinoma) were kept at exponential growth in RPMI 1640 medium with 10% fetal calf serum.[32]

Photosensitization and Cell-Death Determination. Cells (7×10^5 HL60 or 2×10^5 to 3×10^5 4T1) that were seeded in 35 mm dishes were grown overnight at 37 °C and 5% CO_2. Derivatives at a final concentration of 0.01−10 μM were added for 16 h before illumination. Cells were rinsed with PBS, were refed with fresh medium without phenol red for 1 h, and were then illuminated by a 75 W halogen lamp with a band-pass filter (Andover, Salem, NH) with a resulting wavelength of 500−520 nm. The fluence rate at the level of the cell monolayer was 0.7 mW/cm^2, and the total light dose was 2.5 J/cm^2. Following irradiation, the viability of post-PDT cultures was determined the next day by the Trypan blue exclusion method. Control dark experiments (without illumination) were performed in parallel.

DNA Analysis. DNA isolation and analysis from PDT-treated cells were performed as previously described.[32] After being stained with ethidium bromide, DNA was visualized under an electronic dual wave ultraviolet transilluminator (Ultra Lum, Claremont, CA) (365/254 nm).

Confocal Microscopy. We studied the subcellular localization of glycol porphyrin derivatives in 4T1 tumor cells by using CLSM. Cells that were grown on coverslips in 35 mm Petri dishes were incubated with 0.5 μM **2**, **6**, and **10**−**12** and with 5 μM **4**, 7 μM **8**, and 2.5 μM **9** in the complete medium for 16 h. After incubation, cells were loaded with 75 nM MitoTracker Green, 500 nM LysoTracker Green, or 250 nM ER-Tracker Blue-White (Molecular Probes) for 30 min at 37 °C in the complete medium. Cells were washed with PBS three times, were overlaid with media without phenol red, and were examined under a DMI 6000 inverted Leica TCS A0BS SP5 tandem scanning confocal microscope with an Ar (488 nm) laser and a ×100 oil immersion objective. The emission spectra of derivatives were detected between 640 and 700 nm. In the same cells, the emission spectra of green MitoTracker or LysoTracker were detected in the 500−550 nm range, and emission spectra of blue ER-Tracker were detected in the 420−480 nm range. Experiments were repeated three times in minimal ambient light.

Western Immunoblot Analysis. Cellular extracts were prepared 2 h after **2**-, **4**-, **6**-, **8**-, and **9**-mediated PDT, were separated on 10−15% sodium dodecyl sulfate PAGE, and were processed for Western blot analysis as previously described.[49] To determine the MAPK activity, we used phospho-specific antibodies first, and we then stripped the membranes and reprobed them with antibodies to total MAPK. Equal protein loading was verified by Ponceau S staining and actin reprobing. Antibodies that recognized phospho-MKK3/MKK6 (Ser189/207), phospho-p38 MAPK (Thr180/Tyr182), phospho-SAPK/JNK (Thr183/Tyr185), caspase-3, -8, and -9, SAPK/JNK, p38 MAP kinase, MKK3 kinase, and Bcl-2 were from Cell Signaling Technology (Beverly, MA); Mcl-1 (S-19) was from Santa Cruz Biotechnology (Santa Cruz, CA); PARP was purchased from BD Biosciences Pharmingen (San Diego, CA); actin was from Sigma.

Flow Cytometry. HL60 cells (1×10^6) were treated overnight with **2** (200 nM), **4** (3 μM), **6** (250 nM), **8** (6.5 μM), and **9** (2.5 μM) and were illuminated as previously described (2.5 J/cm^2). After 4.5−6.5 h, cells were resuspended in 100 μL of binding buffer and were incubated with both Annexin V and PI for 10 min in the

dark. Then, 10^4 cells were analyzed by a flow cytometer (BD LSRII, FlowJo software). The percentage of live, dead, and apoptotic cells was determined. In the corresponding Figures that illustrate apoptosis, the viable cells (B3) were located in the lower left corner (negative for both Annexin V-FITC and PI). Early apoptotic cells (B4) were in the lower right corner (Annexin V-FITC positive), and late apoptotic cells (B2) were in the upper right corner (positive for both Annexin V-FITC and PI). The total percentage of apoptotic cells was represented as a combination of B2 + B4.

In Vivo Experiments. We made fresh stock solutions of the sensitizers by dissolving the drug in 20 μL of 20% DMSO and adjusting the mixture with water to provide the application dose of 3 mg/kg in a volume of 0.1 mL per 20 g mice. MDA-MB-231cells (1×10^7) that were suspended in 0.1 mL of PBS and 0.1 mL of Matrigel (BD Biosciences, Franklin Lakes, NJ) were injected subcutaneously into hind flanks of the mice. PDT experiments were performed when the tumor mass reached a volume of 100 mm^3 (about 10 days after transplantation). The tumor area (2 cm^2) was irradiated by a 500−700 nm xenon lamp ONL 051 (maximum at 635 nm, Preciosa Crytur, Turnov, Czech Republic) with a total impact energy of 100 J/cm^2 and a fluence rate of 200 mW/cm^2. The tested interval between drug administration and photoirradiation varied from 2 to 72 h. The whole PDT treatment was repeated after 1 week. Tumor dimensions were determined by caliper measurements every third or fourth day after the treatment. The volume of each tumor was calculated as $\pi/6 \times a \times b \times c$ (where a is the longitudinal diameter, b is the short diameter, and c is the thickness). All aspects of the animal experiment and husbandry were carried out in compliance with national and European regulations.

Acknowledgment. This work was funded by projects LC06077 and MSM6046137307 that were awarded by the Ministry of Education of the Czech Republic and by grant 203/06/1038 from the Grant Agency of the Czech Republic. This work was partially supported by project AV0Z50520514 and grant KAN200200651 from the Grant Agency of the Academy of Sciences of the Czech Republic.

Supporting Information Available: The preparations and supporting characterization of compounds **2**−**12** including fluorescence microscopy images of mTHPP (**1a**), pTHPP (**1b**), and ethylene glycol porphyrin derivatives **2** and **6**, confocal microscopy images of **1a**, **2**, **8**−**12**, and mTHPC, titration of **2** and **4** with sialic acid, and absorption spectra of **1a**, **2**, and **10**−**12** at pH 6 and 7.34. This material is available free of charge via the Internet at http://pubs.acs.org.

References

(1) Giovannetti, A.; Pierdominici, M.; Di Iorio, A.; Cianci, R.; Murdaca, G.; Puppo, F.; Pandolfi, F.; Paganelli, R. Apoptosis in the homeostasis of the immune system and in human immune mediated diseases. *Curr. Pharm. Des.* **2008**, *14*, 253–268.

(2) Van Cruchten, S.; Van Den Broeck, W. Morphological and biochemical aspects of apoptosis, oncosis and necrosis. *Anat., Histol., Embryol.* **2002**, *31*, 214–223.

(3) Kroemer, G.; Galluzzi, L.; Brenner, C. Mitochondrial membrane permeabilization in cell death. *Physiol. Rev.* **2007**, *87*, 99–163.

(4) Kaufmann, S. H.; Gores, G. J. Apoptosis in cancer: cause and cure. *BioEssays* **2000**, *22*, 1007–17.

(5) Alkhalaf, M.; El-Mowafy, A.; Renno, W.; Rachid, O.; Ali, A.; Al-Attyiah, R. Resveratrol-induced apoptosis in human breast cancer cells is mediated primarily through the caspase-3-dependent pathway. *Arch. Med. Res.* **2008**, *39*, 162–168.

(6) Balakin, K. V.; Ivanenkov, Y. A.; Kiselyov, A. S.; Tkachenko, S. E. Histone deacetylase inhibitors in cancer therapy: latest developments, trends and medicinal chemistry perspective. *Anti-Cancer Agents Med. Chem.* **2007**, *7*, 576–592.

(7) Danson, S.; Dean, E.; Dive, C.; Ranson, M. IAPs as a target for anticancer therapy. *Curr. Cancer Drug Targets* **2007**, *7*, 785–794.

(8) Díaz-Gavilán, M.; Gómez-Vidal, J. A.; Rodríguez-Serrano, F.; Marchal, J. A.; Caba, O.; Aránega, A.; Gallo, M. A.; Espinosa, A.; Campos, J. M. Anticancer activity of (1,2,3,5-tetrahydro-4,1-benzoxazepine-3-yl)-pyrimidines and -purines against the MCF-7 cell line: preliminary cDNA microarray studies. *Bioorg. Med. Chem. Lett.* **2008**, *18*, 1457–1460.

(9) Dong, L. F.; Swettenham, E.; Eliasson, J.; Wang, X. F.; Gold, M.; Medunic, Y.; Stantic, M.; Low, P.; Prochazka, L.; Witting, P. K.; Turanek, J.; Akporiaye, E. T.; Ralph, S. J.; Neuzil, J. Vitamin E analogues inhibit angiogenesis by selective induction of apoptosis in proliferating endothelial cells: the role of oxidative stress. *Cancer Res.* **2007**, *67*, 11906–11913.

(10) Fulda, S. Inhibitor of apoptosis proteins as targets for anticancer therapy. *Expert Rev. Anticancer Ther.* **2007**, *7*, 1255–1264.

(11) Heikaus, S.; Matuszek, K. S.; Suschek, C. V.; Ramp, U.; Reinecke, P.; Grinstein, E.; Haremza, J.; Gabbert, H. E.; Mahotka, C. Paclitaxel (Taxol)-induced apoptosis in human epithelioid sarcoma cell lines is enhanced by upregulation of CD95 ligand (FasL/Apo-1L). *J. Cancer Res. Clin. Oncol.* **2007**, *134*, 689–695.

(12) Kawanishi, S.; Hiraku, Y. Amplification of anticancer drug-induced DNA damage and apoptosis by DNA-binding compounds. *Curr. Med. Chem.: Anti-Cancer Agents* **2004**, *4*, 415–419.

(13) Kumar, A.; D'Souza, S. S.; Gaonkar, S. L.; Rai, K. M.; Salimath, B. P. Growth inhibition and induction of apoptosis in MCF-7 breast cancer cells by a new series of substituted-1,3,4-oxadiazole derivatives*Invest. New Drugs*, published online Jan 29 2008, http://dx.doi.org/10.1007/s10637-008-9116-5.

(14) Mosley, C. A.; Liotta, D. C.; Snyder, J. P. Highly active anticancer curcumin analogues. *Adv. Exp. Med. Biol.* **2007**, *595*, 77–103.

(15) Russo, A.; Fratto, M. E.; Bazan, V.; Schiro, V.; Agnese, V.; Cicero, G.; Vincenzi, B.; Tonini, G.; Santini, D. Targeting apoptosis in solid tumors: the role of bortezomib from preclinical to clinical evidence. *Expert Opin. Ther. Targets* **2007**, *11*, 1571–1586.

(16) Thongphasuk, P.; Stremmel, W.; Chamulitrat, W. Potent direct or TNF-α-promoted anticancer effects of 2,3-dehydrosilybin: comparison study with silybin. *Chemotherapy* **2008**, *54*, 23–30.

(17) Allison, R. R.; Bagnato, V. S.; Cuenca, R.; Downie, G. H.; Sibata, C. H. The future of photodynamic therapy in oncology. *Future Oncol.* **2006**, *2*, 53–71.

(18) Castano, A. P.; Mroz, P.; Hamblin, M. R. Photodynamic therapy and anti-tumour immunity. *Nat. Rev. Cancer* **2006**, *6*, 535–545.

(19) Wilson, B. C.; Patterson, M. S. The physics of photodynamic therapy. *Phys. Med. Biol.* **1986**, *31*, 327–360.

(20) Henderson, B. W.; Dougherty, T. J. How does photodynamic therapy work? *Photochem. Photobiol.* **1992**, *55*, 145–157.

(21) Niedre, M.; Patterson, M. S.; Wilson, B. C. Direct near-infrared luminescence detection of singlet oxygen generated by photodynamic therapy in cells in vitro and tissues in vivo. *Photochem. Photobiol.* **2002**, *75*, 382–391.

(22) Oleinick, N. L.; Evans, H. H. The photobiology of photodynamic therapy: cellular targets and mechanisms. *Radiat. Res.* **1998**, *150*, S146–S156.

(23) Almeida, R. D.; Manadas, B. J.; Carvalho, A. P.; Duarte, C. B. Intracellular signaling mechanisms in photodynamic therapy. *Biochim. Biophys. Acta* **2004**, *1704*, 59–86.

(24) Oleinick, N. L.; Morris, R. L.; Belichenko, I. The role of apoptosis in response to photodynamic therapy: what, where, why, and how. *Photochem. Photobiol. Sci.* **2002**, *1*, 1–21.

(25) Lavie, G.; Kaplinsky, C.; Toren, A.; Aizman, I.; Meruelo, D.; Mazur, Y.; Mandel, M. A photodynamic pathway to apoptosis and necrosis induced by dimethyl tetrahydroxyhelianthrone and hypericin in leukaemic cells: possible relevance to photodynamic therapy. *Br. J. Cancer* **1999**, *79*, 423–432.

(26) Kessel, D.; Luo, Y.; Deng, Y.; Chang, C. K. The role of subcellular localization in initiation of apoptosis by photodynamic therapy. *Photochem. Photobiol.* **1997**, *65*, 422–426.

(27) Král, V.; Králová, J.; Kaplánek, R.; Bříza, T.; Martásek, P. Quo vadis porphyrin chemistry? *Physiol. Res.* **2006**, *55 (Suppl. 2)*, S3–S26.

(28) Banfi, S.; Caruso, E.; Caprioli, S.; Mazzagatti, L.; Canti, G.; Ravizza, R.; Gariboldi, M.; Monti, E. Photodynamic effects of porphyrin and chlorin photosensitizers in human colon adenocarcinoma cells. *Bioorg. Med. Chem.* **2004**, *12*, 4853–4860.

(29) Samaroo, D.; Vinodu, M.; Chen, X.; Drain, C. M. *meso*-Tetra(pentafluorophenyl)porphyrin as an efficient platform for combinatorial synthesis and the selection of new photodynamic therapeutics using a cancer cell line. *J. Comb. Chem.* **2007**, *9*, 998–1011.

(30) Synytsya, A.; Král, V.; Volka, K.; Sessler, J. L. In vitro interaction of macrocyclic photosensitizers with intact mitochondria: a spectroscopic study. *Biochim. Biophys. Acta* **2003**, *1620*, 85–96.

(31) Král, V.; Rusin, O.; Charvatova, J.; Anzenbacher, P.; Fogl, J. Porphyrin phosphonates: novel anionic receptors for saccharide recognition. *Tetrahedron Lett.* **2000**, *41*, 10147–10151.

(32) Králová, J.; Synytsya, A.; Poučková, P.; Koc, M.; Dvořák, M.; Král, V. Novel porphyrin conjugates with a potent photodynamic antitumor effect: differential efficacy of mono- and bis-beta-cyclodextrin derivatives in vitro and in vivo. *Photochem. Photobiol.* **2006**, *82*, 432–438.

(33) Rusin, O.; Hub, M.; Král, V. Novel water-soluble porphyrin-based receptors for saccharide recognition. *Mater. Sci. Eng., C* **2001**, *18*, 135–140.
(34) Sibrian-Vazquez, M.; Jensen, T. J.; Vicente, M. G. Synthesis and cellular studies of PEG-functionalized *meso*-tetraphenylporphyrins. *J. Photochem. Photobiol., B* **2007**, *86*, 9–21.
(35) Crupi, V.; Giordano, R.; Majolino, D.; Migliardo, P.; Venuti, V.; Micali, N.; Villari, V.; Mineo, P.; Vitalini, D.; Scamporrino, E. Spectroscopic evidence of aggregation processes in porphyrin-based star-polymers in agueous solutions. *Mol. Phys.* **2003**, *101*, 1517–1526.
(36) Swamy, N.; Purohit, A.; Fernandez-Gacio, A.; Jones, G. B.; Ray, R. Nuclear estrogen receptor targeted photodynamic therapy: selective uptake and killing of MCF-7 breast cancer cells by a C17α-alkynylestradiol-porphyrin conjugate. *J. Cell. Biochem.* **2006**, *99*, 966–977.
(37) Tkadlecova, M.; Foltynova, J.; Valik, M.; Král, V. Spectroscopic binding studies of novel fluorescent distamycin derivatives. *Tetrahedron Lett.* **2008**, *49*, 323–326.
(38) Kobayashi, N.; Nakai, K. Application of magnetic circular dichroism spectroscopy to porphyrins and phthalocyanines. *Chem. Commun.* **2007**, *40*, 4077–4092.
(39) Surewicz, W. K. Electron spin resonance study on the mechanism of polyethylene glycol-membrane interaction. *FEBS Lett.* **1983**, *151*, 228–232.
(40) Kirk, K. L. Fluorine in medicinal chemistry: recent therapeutic applications of fluorinated small molecules. *J. Fluorine Chem.* **2006**, *127*, 1013–1029.
(41) Weitman, H.; Schatz, S.; Gottlieb, H. E.; Kobayashi, N.; Ehrenberg, B. Spectroscopic probing of the acid-base properties and photosensitization of a fluorinated phthalocyanine in organic solutions and liposomes. *Photochem. Photobiol.* **2001**, *73*, 473–481.
(42) Biffinger, J. C.; Kim, H. W.; DiMagno, S. G. The polar hydrophobicity of fluorinated compounds. *ChemBioChem* **2004**, *5*, 622–627.
(43) Kim, D.; Wang, L.; Beconi, M.; Eiermann, G. J.; Fisher, M. H.; He, H.; Hickey, G. J.; Kowalchick, J. E.; Leiting, B.; Lyons, K.; Marsilio, F.; McCann, M. E.; Patel, R. A.; Petrov, A.; Scapin, G.; Patel, S. B.; Roy, R. S.; Wu, J. K.; Wyvratt, M. J.; Zhang, B. B.; Zhu, L.; Thornberry, N. A.; Weber, A. E. (2*R*)-4-oxo-4-[3-(trifluoromethyl)-5,6-dihydro[1,2,4]triazolo[4,3-*a*]pyrazin−7(8*H*)-yl]-1-(2,4,5-trifluorophenyl)butan-2-amine: a potent, orally active dipeptidyl peptidase IV inhibitor for the treatment of type 2 diabetes. *J. Med. Chem.* **2005**, *48*, 141–151.
(44) Králová, J.; Dvořák, M.; Koc, M.; Král, V. p38 MAPK plays an essential role in apoptosis induced by photoactivation of a novel ethylene glycol porphyrin derivative. *Oncogene* **2008**, *27*, 3010–3020.
(45) Hirohara, S.; Obata, M.; Ogata, S.; Ohtsuki, C.; Higashida, S.; Ogura, S.; Okura, I.; Takenaka, M.; Ono, H.; Sugai, Y.; Mikata, Y.; Tanihara, M.; Yano, S. Cellular uptake and photocytotoxicity of glycoconjugated chlorins in HeLa cells. *J. Photochem. Photobiol., B* **2005**, *78*, 7–15.
(46) Banfi, S.; Caruso, E.; Buccafurni, L.; Murano, R.; Monti, E.; Gariboldi, M.; Papa, E.; Gramatica, P. Comparison between 5,10,15,20-tetraaryl- and 5,15-diarylporphyrins as photosensitizers: synthesis, photodynamic activity, and quantitative structure-activity relationship modeling. *J. Med. Chem.* **2006**, *49*, 3293–3304.
(47) Fabris, C.; Valduga, G.; Miotto, G.; Borsetto, L.; Jori, G.; Garbisa, S.; Reddi, E. Photosensitization with zinc (II) phthalocyanine as a switch in the decision between apoptosis and necrosis. *Cancer Res.* **2001**, *61*, 7495–7500.
(48) Dougherty, T. J.; Gomer, C. J.; Henderson, B. W.; Jori, G.; Kessel, D.; Korbelik, M.; Moan, J.; Peng, Q. Photodynamic therapy. *J. Natl. Cancer Inst.* **1998**, *90*, 889–905.
(49) Králová, J.; Dvořák, M.; Král, V. Novel cationic transport agents for oligonucleotide delivery into primary leukemic cells. *J. Med. Chem.* **2003**, *46*, 2049–2056.

JM8002119